Remote sensing of the chlorophyll-*a* based on OLI/Landsat-8 and MSI/Sentinel-2A (Barra Bonita reservoir, Brazil)

FERNANDA WATANABE[1], ENNER ALCÂNTARA[2], THANAN RODRIGUES[1], LUIZ ROTTA[1], NARIANE BERNARDO[1] and NILTON IMAI[1]

[1]Department of Cartography, São Paulo State University,
Rua Roberto Simonsen, 305, 19060-900 Presidente Prudente, SP, Brazil
[2]Department of Environmental Engineering, São Paulo State University, Rodovia
Presidente Dutra, Km 137,8, 12247-004 São José dos Campos, SP, Brazil

ABSTRACT

In this present research, we assessed the performance of band algorithms in estimating chlorophyll-*a* (Chl-*a*) concentration based on bands of two new sensors: Operational Land Imager onboard Landsat-8 satellite (OLI/Landsat-8), and MultiSpectral Instrument onboard Sentinel-2A (MSI/Sentinel-2A). Band combinations designed for Thematic Mapper onboard Landsat-5 satellite (TM/Landsat-5) and MEdium Resolution Imaging Spectrometer onboard Envisat platform (MERIS/Envisat) were adapted for OLI/Landsat-8 and MSI/Sentinel-2A bands. Algorithms were calibrated using *in situ* measurements collected in three field campaigns carried out in different seasons. The study area was the Barra Bonita hydroelectric reservoir (BBHR), a highly productive aquatic system. With exception of the three-band algorithm, the algorithms were spectrally few affected by sensors changes. On the other hands, algorithm performance has been hampered by the bio-optical difference in the reservoir sections, drought in 2014 and pigment packaging.

Key words: algal bloom, inland water color, spectral index, water quality, satellite imagery.

INTRODUCTION

Retrieving the concentration of optically significant constituents (OSCs) is a challenge for the remote sensing of water color. Band algorithms have been widely used due to simple implementation and calibration based on statistical regression between reflectance data and water quality parameters of

Correspondence to: Fernanda Sayuri Yoshino Watanabe
E-mail: fernandasyw@gmail.com

* Contribution to the centenary of the Brazilian Academy of Sciences.

interest. Several band combinations were designed using different band quantities and structure (Carder et al. 1999, Dall'Olmo et al. 2005, Le et al. 2009, Mishra and Mishra 2010, 2012). These algorithms are better suited to environmental monitoring by satellite, which needs quick results for decision-making, therefore the empirical approaches can be quickly and easily implemented. However, the empirical approach has the disadvantage of being limited to a geographic location and a seasonal regime (Moses et al. 2012). Despite of that, the

band combination may be appropriate for other aquatic systems, being need only calibration.

Initially, the algorithms for estimating chlorophyll-*a* (Chl-*a*) were originally developed for marine waters using bands at the blue and green regions of the electromagnetic spectrum (Aiken et al. 1995, Clark, 1997, Carder et al. 1999). However, in inland waters those algorithms are inappropriate due to the high colored dissolved organic matter (CDOM), which absorbs strongly in the blue region, masking the Chl-*a* absorption (Carder et al. 1999, Mannino et al. 2008). Additionally, atmospheric influence is higher at shorter wavelengths (ultraviolet and blue region) (Gordon et al. 1988, Siegel et al. 2000), hampering the performance of models using blue band (Mannino et al. 2008). Inland waters such as lakes and reservoirs undergo with high eutrophication level and toxic phytoplankton bloom (Tundisi et al. 2008, Dantas et al. 2011, Oliveira et al. 2014).

Most of algorithms were designed for specific sensors such as MERIS, Moderate Resolution Imaging Spetroradiometer (MODIS), Sea-viewing Wide Field-of-view Sensor (SeaWiFS) and sensors of Landsat mission. Considering the smaller dimension of freshwater bodies such as rivers and reservoirs, MERIS and Landsat sensors were the most suitable, due to their higher spatial resolution. However, MERIS sensor stopped transmitting data in 2011 and, in the next year, Thematic Mapper from Landsat-5 (TM/Landsat-5) became non-operational. There was a lack of images for inland water applications until the launch of the Operational Land Imager (OLI) sensor onboard Landsat-8 satellite in February 2014 (NASA, https://www.nasa.gov/). In turn, the MultiSpectral Instrument (MSI) onboard Sentinel-2A satellite was launched in June 2015 (ESA, http://www.esa.int/ESA). Now with availability of both sensors data, several researches have been conducted in order to extract information for water color applications such as optical properties and OSCs (Watanabe et

al. 2015). In this context, the goal of this research was to evaluate the performance of OLI/Landsat-8 and MSI/Sentinel-2A sensors-based empirical algorithms in estimating Chl-*a* concentration in a tropical productive reservoir. The spectral indexes tested were based on those designed for TM/Landsat-5 and MERIS/Envisat images in order to retrieve Chl-*a* in productive waters. Due to some changes in the band setting of the sensors, small adaptations were conducted in the spectral indexes, for instance, the MSI/Sentinel-2A band centered at 709 nm was replaced for 705 nm.

MATERIALS AND METHODS

STUDY AREA AND FIELD SURVEY

The Barra Bonita hydroelectric reservoir (BBHR) (22º31'10"S and 48º32'3"W) is located in the middle course of the Tietê River, in São Paulo State, Brazil (Figure 1). The flooded area is of 310 km^2, with volume of approximately 3.622 x 10^6 m^3 whereas the quota ranges from 439.5 m to 451.5 m (AES Tietê, http://www.aestiete.com.br/). The average depth is 10.2 m with a maximum of 25 m (Tundisi et al. 2008). The flow varies from 200 m^3 s^{-1} in the dry season (austral winter) to 1,500 m^3 s^{-1} in the rainfall season (austral summer), while the retention time ranges from 30 days (austral summer) to 180 days (austral winter) (Matsumura-Tundisi and Tundisi 2005). The BBHR is the first dam of six reservoirs cascading in the Tietê River. The BBHR presents a high eutrophication level due to the wastewater discharge coming from the São Paulo metropolitan area. The region is characterized by a wet period between November and April and drought from May to October (Matsumura-Tundisi and Tundisi 2005).

Three field campaigns were conducted in the BBHR: two field surveys for collecting calibration dataset and one for validation dataset. Radiometric measures and water samples were acquired to estimate concentrations of Chl-*a* as well as total,
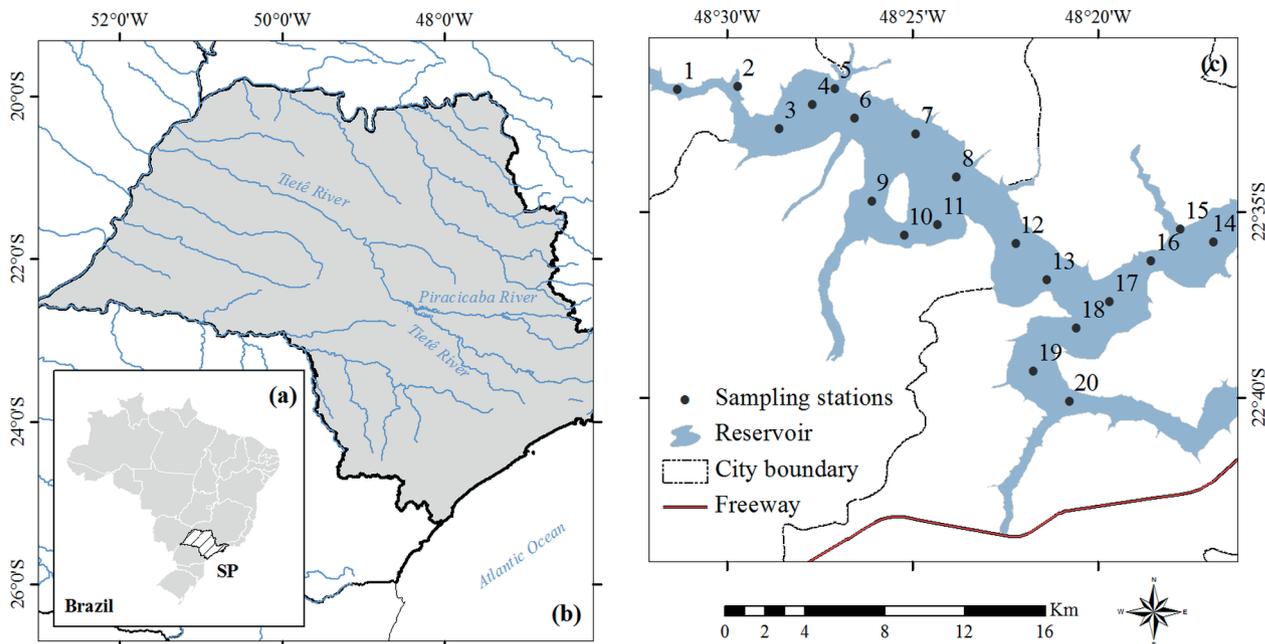
Figure 1 - Study area. (**a**) Location of São Paulo State in Brazil. (**b**) Position of the Piracicaba and Tietê rivers in hydrographical network in São Paulo State. (**c**) Barra Bonita hydroelectric reservoir (BBHR) and distribution of the sampling stations along the reservoir.

organic and inorganic suspended solids (TSS, ISS and OSS, respectively). Approximately 5 liters of water samples were collected at each sampling point. The samples were stored in sterile plastic bottles, and kept cold and in dark environment until filtration. Measurements of turbidity and Secchi disk depth (SDD) were also collected. The first calibration field campaign was conducted on May 5 – 9, 2014 (austral autumn), while the second was carried out on October 13 – 16, 2014 (austral spring). The validation field survey was carried out on September 13 – 15, 2015 (austral winter). These dates were selected to match periods of low rainfall and Landsat-8 satellite overpass.

REMOTE SENSING REFLECTANCE

The remote sensing reflectance, R_{rs} (in sr^{-1}), was derived from radiometric data measured above the surface and calculated using Equation 1 proposed by Mobley (1999).

$$R_{rs}(\lambda) = \frac{L_t(\lambda) - \rho L_{sky}(\lambda)}{E_s(\lambda)} \tag{1}$$

where L_t (W·m^{-2}·sr^{-1}) is the total radiance, i.e., the sum of water-leaving spectral radiance (L_w, in W·m^{-2}·sr^{-1}) and reflected radiance from the water surface in the direction of the sensor (L_r, in W·m^{-2}·sr^{-1}); the influence of L_r is corrected from the incident sky radiance (L_{sky}, in W·m^{-2}·sr^{-1}); surface reflectance factor ($\rho = 0.028$) (Mobley 1999) and E_s (W·m^{-2}) is the irradiance incident onto water surface.

Three RAMSES spectroradiometers (TriOS, Rastede, Germany) were used to measure the radiometric quantities required for the calculation of the R_{rs}. E_s was measured using a cosine collector, ACC-VIS RAMSES sensor, whereas L_t and L_{sky} were measured using two ARC-VIS RAMSES sensors, with a 7° FOV in air. The ACC-VIS and ARC-VIS work in a range of 320 to 950 nm with a spectral sampling and accuracy of 3.3 nm and 0.3 nm, respectively. The operational temperature range

is between -10 ºC and +50 ºC with water resistance of 300 m. Radiometric data were collected using geometric acquisition proposed by Mobley (1999) and Mueller (2003). The cosine collector was pointed in an upward direction for collecting the incident spectral irradiance, $E_s(\lambda)$. The sensor was coupled to a structure of approximately 1.5 m to avoid shadows. One of the ARC-VIS sensors was pointed in an upward direction of 45º in relation to the zenith to measure the incident sky radiance, $L_{sky}(\lambda)$. Another radiance sensor was pointed in a downward direction of 45º in relation to nadir position to measure the surface radiance, $L_t(\lambda)$. All the sensors collected the measurements simultaneously.

CONCENTRATIONS OF OSCS

The collected water samples were filtered through a Whatman GF/F glass fiber filter, with 0.7 μm size pore and 47 mm diameter, to estimate Chl-*a* and particulate material concentration. A vacuum pressure pump and a filter holder were used in the filtration. Due to the high concentration of solids in the BBHR, a very small volume (250 mL) was filtered at each filtration. Filters with retained material were stored, frozen and in the dark, until analysis. Extraction by the acetone method was used to estimate Chl-*a* concentration (Golterman 1975). Chl-*a* was extracted using 90% acetone solution. Sample absorbance was measured at wavelengths of 663 nm and 750 nm using a spectrophotometer and a cuvette with 1 cm path length. The samples were afterwards acidified using a 0.1 N hydrochloric acid (HCl) solution to correct the interference of phaeophytin. Meanwhile, concentrations of TSS, OSS, and ISS were estimated using the 2540 Solids method proposed by APHA (1998, p. 2-54).

CALIBRATION OF EMPIRICAL MODELS

Existing models were fitted taking into account OLI/Landsat-8 and MSI/Sentinel-2A bands. Bands of those sensors were simulated from in situ data and used to calibrate and validate models for Chl-*a* estimation. The simulation of bands was carried out from *in situ* R_{rs} measurements and the spectral response function of each sensor (Barsi et al. 2014, ESA 2015), using Equation 2 (Van der Meer 1999).

$$R_{rs,k} = \frac{\int_{\lambda_{1k}}^{\lambda_{2k}} R_{rs}(\lambda,t) S_k(\lambda) d\lambda}{\int_{\lambda_{1k}}^{\lambda_{2k}} S_k(\lambda) d\lambda} \qquad (2)$$

where, $S_k(\lambda)$ is the radiometric sensitivity of band k, whose band width is from wavelength λ_{1k} to λ_{2k} ($\lambda_{1k} < \lambda_{2k}$).

Simulated bands were used to test empirical models proposed by different authors to estimate the Chl-*a* concentration in BBHR. Empirical models were calibrated from spectral indexes proposed by different authors. Different band combinations were tested using two and three bands. Two-band (2B) and three-band (3B) models (Equation 3 and 4), originally developed to estimate Chl-*a* in terrestrial vegetation (Gitelson et al. 2003) and later adapted by authors for Chl-*a* algal in aquatic systems. In both models, the first band position λ_1 must be maximally sensitive to absorption by Chl-*a* (a_φ). To minimize the absorption effects of other OSCs, a second spectral band λ_2 is used, which must be minimally sensitive to a_φ, and present absorption by non-algal particles and CDOM, (a_{NAP} and a_{CDOM}, respectively), similar to the finding at λ_1. 2B is still affected by backscattering (b_b), which can produce different Chl-*a* estimates for locations with equal concentration. A third band, λ_3, can be used in order to minimize the b_b influence, where absorption must be associated only with pure water (Gitelson et al. 2008).

$$2B = \left[R_{rs}^{-1}(\lambda_1) \times R_{rs}(\lambda_2) \right] \qquad (3)$$

$$3B = \left[R_{rs}^{-1}(\lambda_1) - R_{rs}^{-1}(\lambda_2) \right] \times R_{rs}(\lambda_3) \qquad (4)$$

The slope model (Equation 5), developed by Mishra and Mishra (2010) for turbid waters based on the red and green bands of the MODIS sensor, was also tested. The Slope index represents the variation rate of reflectance from $R_{rs}(\lambda_2)$ to $R_{rs}(\lambda_1)$ in relation to the wavelengths λ_2 to λ_1. The wavelength λ_1 is associated with minimum absorption by Chl-*a*, while λ_2 is related to maximum absorption.

$$Slope = \frac{R_{rs}(\lambda_2) - R_{rs}(\lambda_1)}{\lambda_2 - \lambda_1} \qquad (5)$$

Finally, the Normalized Difference Chlorophyll Index (NDCI) developed by Mishra and Mishra (2012), based on MERIS bands for applications in estuarine and coastal turbid productive waters (Equation 6), was tested. Similar to the Normalized Difference Vegetation Index (NDVI), the first band position λ_1 is associated with maximally sensitive Chl-*a* in the red spectral region, while the second position λ_2 meets the band of minimally sensitive Chl-*a* in NIR region, in this case at 709 nm.

$$NDCI = \frac{R_{rs}(\lambda_2) - R_{rs}(\lambda_1)}{R_{rs}(\lambda_2) + R_{rs}(\lambda_1)} \qquad (6)$$

In OLI models, green (560 nm) and red bands (655 nm) were used as λ_1 and λ_2, respectively (Mishra and Mishra 2010, 2012), whilst MSI models, bands in red (665 nm), red-edge (705 nm) and NIR (740 nm) were used as λ_1, λ_2 and λ_3, respectively (Gitelson et al. 2008). All the models were calibrated using the least square method, testing linear and polynomial (second degree) adjustments. A prediction interval was taken into account, with a confidence level of 0.95, to calibrate the models. Samples positioned out of the prediction interval were considered as outliers and removed from the models.

CHL-*A* MAPPING

The fieldworks were carried out to coincide with OLI/Landsat-8 images in order to map the Chl-*a* using a model calibrated for the bands of the OLI sensor. However, a unique OLI/Landsat-8 image was acquired on October 13th, 2014 in suitable conditions (without clouds). Before algorithm application, two products were tested: Landsat 8 Surface Reflectance (L8SR) (USGS, http://landsat.usgs.gov/CDR_LSR.php) and at-surface reflectance (R_{sup}) computed by Fast Line-of-sight Atmospheric Analysis of Spectral Hypercubes) (Adler-Golden et al. 1998). Both L8SR and R_{sup} were converted into R_{rs} dividing them by π. To choose the most appropriate product an optical closure was conducted to check the matching between simulated R_{rs} from *in situ* dataset and L8SR product. Studies have shown high quality estimative in aquatic systems using L8SR product (Pahlevan et al. 2017, Bernardo et al. 2017). The comparison was carried out from five measurements collected precisely on the day of satellite overpass. Finally, the best models calibrated for OLI bands were applied to the corrected image.

VALIDATION

A 24-sample dataset collected on September 13-15, 2015 was used to validate the empirical models. The statistical metrics used were: Root Mean Square Error (RMSE – Equation 7); Normalized Root Mean Square Error (NRMSE – Equation 8); Mean Absolute Percentage Error (MAPE – Equation 9); bias (Equation 19); and determination coefficient (R^2).

$$RMSE = \sqrt{\frac{1}{n} \sum_{i=1}^{n} \left(y_i' - y_i \right)^2} \qquad (7)$$

$$NRMSE = \frac{RMSE}{y_{max} - y_{min}} \qquad (8)$$

$$MAPE = \frac{\sum_{i=1}^{n} \left(\frac{\left| y_i' - y_i \right|}{y_i} \right)}{n} \qquad (9)$$

$$bias = \frac{1}{n}\sum_{i=1}^{n}\left(y_i^{'} - y_i\right) \quad (10)$$

where, y_{max} is the maximum measured value; y_{mim} is the minimum measured value; $y_i^{'}$ are predicted values; y_i are measured values; and n is the number of samples.

RESULTS

WATER QUALITY PARAMETERS

Table I shows a summary of the water quality parameters collected along three field campaigns accomplished in BBHR. Analyzing Table I, the difference between values exhibited for each parameter in different months can be noticed.

The month of October presented the highest values for all parameters. Along the three fieldworks, BBHR exhibited high Chl-*a* concentrations, from which it is possible to classify it as a eutrophic environment (Chl-*a* > 60 mg m^{-3}) (Vollenweider and Kerekes 1980). October exhibited especially high concentrations of Chl-*a* (up to 797.8 mg m^{-3}), due to the below average rainfall in 2014 (Coelho et al. 2016, Getirana 2016, Watanabe et al. 2016, INMET, http://www.inmet.gov.br/portal/), causing a remarkable decrease in the water levels in the São Paulo State reservoirs and leading to a water supply crisis in some cities, and harming the commodity transportation via navigation. Hence, there was a greater water flow control in reservoirs, leading to an increase of time retention, contributing to the development of algal communities (Tundisi et al. 2008). According to SDD, the BBHR can be considered as eutrophic, with values less than 1.1 m (Carlson 1977).

During data surveying, the presence of algal cells and filaments sparsely distributed in the water column was noted, making the measurements of turbidity difficult. In other words, there was a remarkable variation among the turbidity readings, because the beam was more attenuated

TABLE I
Descriptive statistics of the water quality parameters measured in the field campaigns carried out in May 2014 (*n* = 18 samples), October 2014 (*n* = 20 samples) and September 2015 (*n* = 24 samples). Statistical metrics used were: minimum value (Min), maximum value (Max), mean and standard deviation (SD).

		May 2014	Oct 2014	Sep 2015
Chl-*a*, mg m^{-3}	Min – Max	17.7 – 279.9	263.2 – 797.8	62.8 – 245.7
	Mean (SD)	120.4 (70.3)	428.7 (154.5)	127.1 (51.3)
TSS, g m^{-3}	Min – Max	3.6 – 16.3	10.8 – 44.0	16.6 – 22.0
	Mean (SD)	7.2 (3.3)	22 (7.0)	17.6 (1.1)
OSS/TSS, %	Min – Max	45 – 98	78 – 96	-
	Mean (SD)	83 (12)	87 (5.0)	-
ISS/TSS, %	Min – Max	2 – 55	4.0 – 22.0	-
	Mean (SD)	17 (12)	13.0 (5.0)	-
TSS:Chl-*a*, g mg^{-1}	Min – Max	0.036 – 0.248	0.029 – 0.077	0.016 – 0.088
	Mean (SD)	0.074 (0.048)	0.054 (0.015)	0.047 (0.014)
Turbidity, NTU	Min – Max	1.7 – 12.5	11.6 – 33.2	3.1 – 6.8
	Mean (SD)	5.2 (2.4)	18.6 (5.3)	4.2 (0.8)
SDD, m	Min – Max	0.8 – 2.3	0.4 – 0.8	1.0 – 1.6
	Mean (SD)	1.5 (0.4)	0.6 (0.1)	1.3 (0.2)

in some samplings and less in others. Hence, three measurements were acquired at each sampling point and the average of the measures was used. In addition, it was noted that TSS was mainly composed of OSS, with a mean portion of 90%. Chl-*a* and OSS presented a positive correlation of approximately 0.82. Although October presented the highest Chl-*a* and OSS concentrations, correlation between both was low in this month, at about 0.33, while in May the correlation was 0.75. The low correlation in October can be

strongly linked to pigment packaging due to high phytoplankton growth (Alcântara et al. 2016).

CHL-*A* RETRIEVAL ALGORITHMS

Figure 2 illustrates the R_{rs} spectra collected in May and October 2014, and September 2015 (Fig. 2a, 2b and 2c, respectively) and simulated bands for OLI/Landsat-8 (Fig. 2d, 2e and 2f) and MSI/Sentinel-2A (Fig. 2g, 2h and 2i) sensors. It is clear the loss of the spectral detailing with the simulated bands. At first, we notice the lack of the reflectance peak around

715 nm associated with scattering of particles in simulated OLI/Landsat-8 bands, followed by the absence of the absorption and fluorescence features of phycocyanin pigment around 620 and 650 nm, respectively, for both sensors.

The linear relationship between the Chl-*a* and spectral indexes for calibration data and OLI bands are shown in Figure 3a and 3b. R^2 lower than 1%, suggesting no correlation between 2O index and Chl-*a* concentration for BBHR, indicate that these indexes are not sufficient for Chl-*a* estimate models
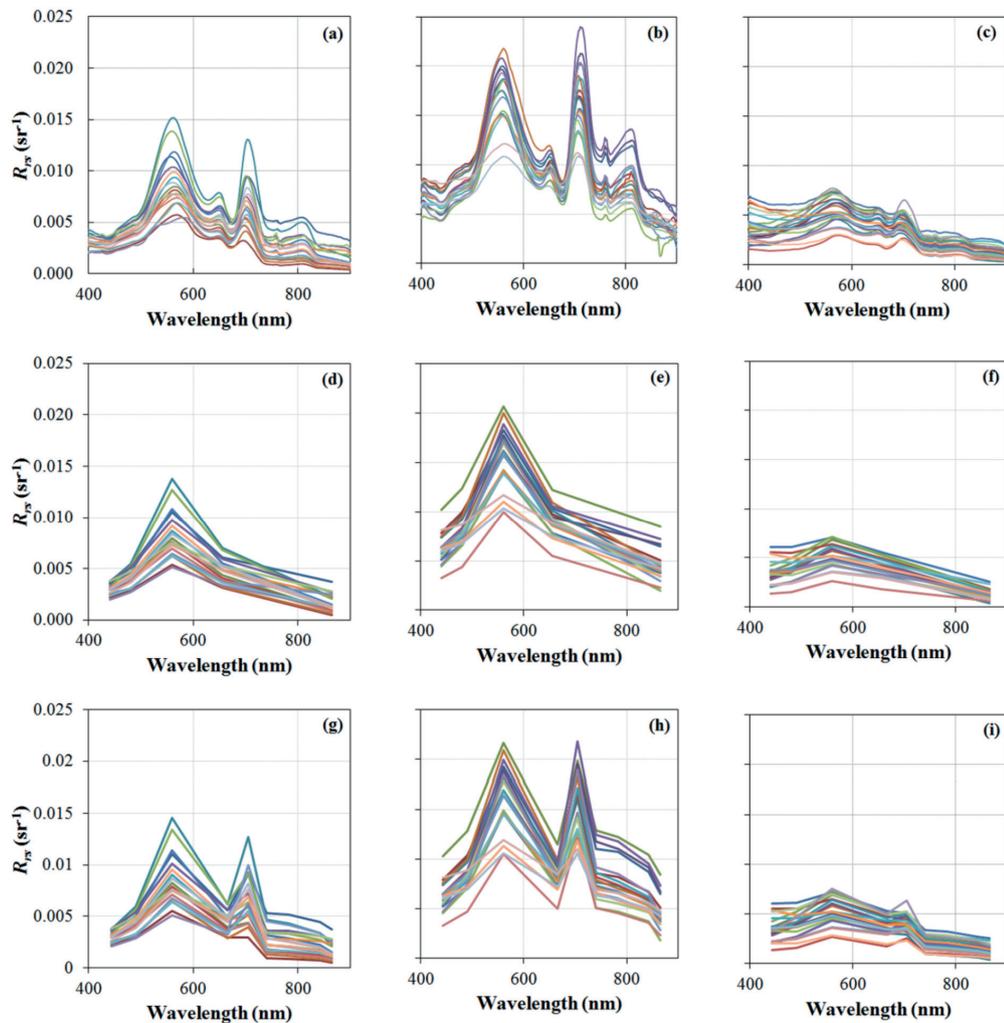

Figure 2 - Remote sensing reflectance spectra acquired in (**a**) May 2014, (**b**) October 2014, and (**c**) September 2015. Simulated R_{rs} spectra for OLI/Landsat-8 based on data collected in (**d**) May, (**e**) October 2014 and (**f**) September 2015 and MSI/Sentinel-2A based on data collected in (**g**) May, (**h**) October 2014 and (**i**) September 2015.

in BBHR. As expected, the optical complexity of inland waters, with solute and particle inputs coming from the drainage basin, impairs the use of shorter wavelengths, strongly influenced by different OSCs. Despite this, even using the same bands of 2O index, the Slope structure considerably improved the relationship with Chl-a, increasing R^2 to 0.78. In this case, the Slope can be seen as the derived value in that spectral range (560 – 665 nm), minimizing multiple effects of OSC such as TSS and highlighting the Chl-a feature (Goodin et al. 1993).

Plots between the Chl-a and spectral indexes proposed for applications to MSI/Sentinel-2A bands are presented in Figures 3c to 3f. The indexes of two bands presented satisfactory correlation with Chl-a (R = 0.859 for 2MSI, R = 0.832 for NDCI and R = 0.902 for SLMSI), showing that the replacement of the wavelength at 560 nm by 709 nm improves the Chl-a estimation, in BBHR. 3MSI index also showed a satisfactory correlation with Chl-a (R = 0.915), corroborating the evidence that NIR-red combination produces high correlation with Chl-a. However, the insertion of 754 nm did not improve the relation with Chl-a, likely due to low b_b for non-algal particles in NIR.

As expected, the 2O index proposed for clear waters was not statistically significant to explain Chl-a concentration in the BBHR (R^2 = 5.43 and p-value = 0.19 for linear fit and R^2 = 7.35% and p-value = 0.32 for 2nd degree fit). Of the fits using OLI bands, the SLO exhibited the best adherence (R^2 = 60.1% and p-value < 0.000 for linear fit and R^2 = 60.3% and p-value < 0.000) for quadratic fit, while simple band ratios using the same bands presented expressionless R^2 values of 5.4% to 7.4% (linear and quadratic fits, respectively).

Among the adjustments based on MSI/Sentinel-2A bands, the calibrations for SLMSI index exhibited the best performance (R^2 = 81.4% and p-value < 0.000 for linear fit, and R^2 = 81.9% and p-value < 0.000 for 2nd degree fit). Following,

the algorithms fitted based on 2MSI index showed satisfactory adherence (R^2 = 73.8% and p-value < 0.000 for linear fit and R^2 = 75.3% and p-value < 0.000 for 2nd degree fit). Algorithms fitted for 3MSI (R^2 of 69.4% and p-value < 0.000 for linear fit and R^2 = 70.5% and p-value < 0.000 for 2nd degree fit) and NDCI indexes (R^2 of 69.2% and p-value < 0.000 for linear fit and R^2 = 71.3% and p-value < 0.000 for 2nd degree fit) exhibited similar adherence. In this case, the insertion of 754 nm did not show improvement in prediction algorithm, most likely due to low b_b of non-algal particles in the BBHR.

SLO (2nd degree fit) algorithm exhibited the second lowest errors (NRSME = 46.4% and MAPE = 47.1%) (Table II). Despite that, R^2 were very low for both the algorithms (< 22%). Meanwhile, validation showed that all the algorithms for Sentinel-2A bands presented similar errors. Despite that, some indexes produced negative estimates such as NDCI indexes (linear fit) which highlighted with the lowest errors (NRMSE = 40.2% and MAPE = 57.4%). On the other hand, 2MSI (2nd degree fit) algorithm exhibited similar performance (NRMSE = 43.9% and MAPE = 58.2%), but there was no problem of negative predictions. Overall, the indexes based only on 665 nm and 709 nm exhibited the best results, corroborating that the insertion of 754 nm do not improve the Chl-a estimation in BBHR. SLMSI index (linear fit) also exhibited good results, with the lowest MAPE (49.02%) and underestimation (bias = 65.02 mg m^{-3}).

Analyzing the results, it was noticed that the algorithms underestimated the Chl-a for both OLI/Landsat-8 and MSI/Sentinel-2A bands, indicating, once again, that empirical algorithms are limited for application in specific period. Overall, the algorithms showed a poorer performance for higher Chl-a concentrations, indicating that pigment packaging affects the algorithm performance. Further, the September dataset exhibited values of Chl-a, which can be negatively affected the SLO
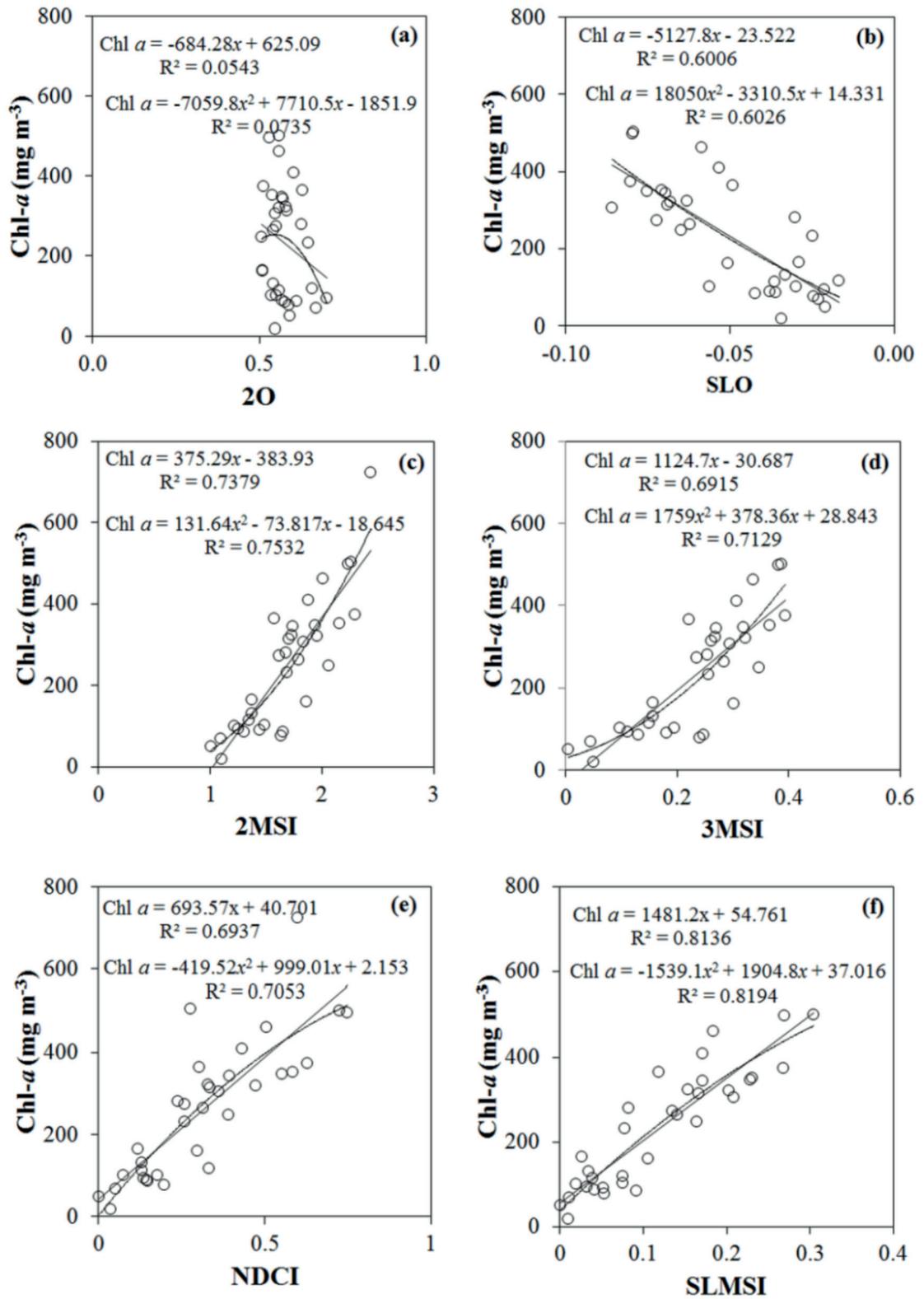
Figure 3 - Models of retrieving Chl-*a* using OLI/Landsat-8 bands and considering the spectral indexes (**a**) 2O and (**b**) SLO, and MSI/Sentinel-2A bands and indexes (**c**) 2MSI, (**d**) 3MSI, (**e**) NDCI and (**f**) SLMSI

TABLE II
Validation of the models considering RMSE, NRMSE, MAPE, bias and R^2 for OLI and MSI.

Index	Fit	RMSE (mg·m^{-3})	NRMSE (%)	MAPE (%)	Bias (mg·m^{-3})	R^2 (%)
Validation of the models calibrated using OLI bands						
SLO	1st	100.56	54.97	61.70	-84.62	0.01
SLO	2nd	84.95	46.44	47.14	-66.86	0.02
Validation of the models calibrated using MSI bands						
2MSI	1st	111.50	69.65	98.57	-109.28	83.67
2MSI	2nd	75.13	43.85	58.18	-71.11	83.45
3MSI	1st	127.41	37.85	115.86	-122.86	84.34
3MSI	2nd	80.21	55.49	64.73	-77.31	84.94
NDCI	1st	69.24	40.62	57.41	-65.97	82.49
NDCI	2nd	101.51	47.71	90.68	-97.68	81.68
SLMSI	1st	74.31	69.65	49.02	-65.02	76.12
SLMSI	2nd	87.28	43.85	64.59	-80.92	76.04

performance. Its dependence to shorter wavelengths (green band) became the model more sensible to dataset than MSI/Sentinel-2A models.

The SLO model using quadratic fit was applied to an OLI/Landsat-8 image acquired on October 13th, 2014, in which the map of Chl-*a* concentration is illustrated in Figure 4. The model was applied in L8SR product, which showed a better matching with *in situ* R_{rs} (Bernardo et al. 2017). Comparing the Chl-*a* range in the map and collected *in situ*, the underestimation in the model is apparent; however, it better represented the Chl-*a* range and distribution in BBHR. Although SLO has not shown the best validation results, the fit was statistically significant (*p*-value = 0.000) and its application on the image from October 2014, matching with the fieldwork date, was performed satisfactorily.

DISCUSSION

P3 presented other different bio-optical status such the lowest dissolved organic carbon (DOC) concentration of 1.04 mg L^{-1}, while the mean in the reservoir was of 10.1 mg L^{-1} (Table I). Furthermore, the fact that the highest Chl-*a* concentration values have been pointed as outliers also can be associated with pigment packaging or self-shading (Alcântara et al. 2016). The packing effect can lead to flattening the absorption coefficient spectra (Bricaud et al. 1995, Carder et al. 1999, Ciotti et al. 2002). So, even though Chl-*a* concentrations increase, the Chl-*a* features are not still more highlighted in the absorption spectra, leading to underestimation of high concentrations. P3 is next to the dam, located before the channel narrows in the lacustrine zone. This region showed rather favorable conditions for algal blooms mainly due to high residence time (Prado and Novo 2015) and sewage discharge into the water, which increases the nutrients concentrations (see location on Fig. 1). Historically, the BBHR always was considered a eutrophic environment, however, in 2014 an extreme drought event caused an intense algal bloom (Coelho et al. 2016, Getirana 2016, Watanabe et al. 2016), contributing for package effect.

Furthermore, the underestimation of the model can also be related to pigment package effect, in which the Chl-*a* concentration increases, but the absorption by Chl-*a* does not (Alcântara
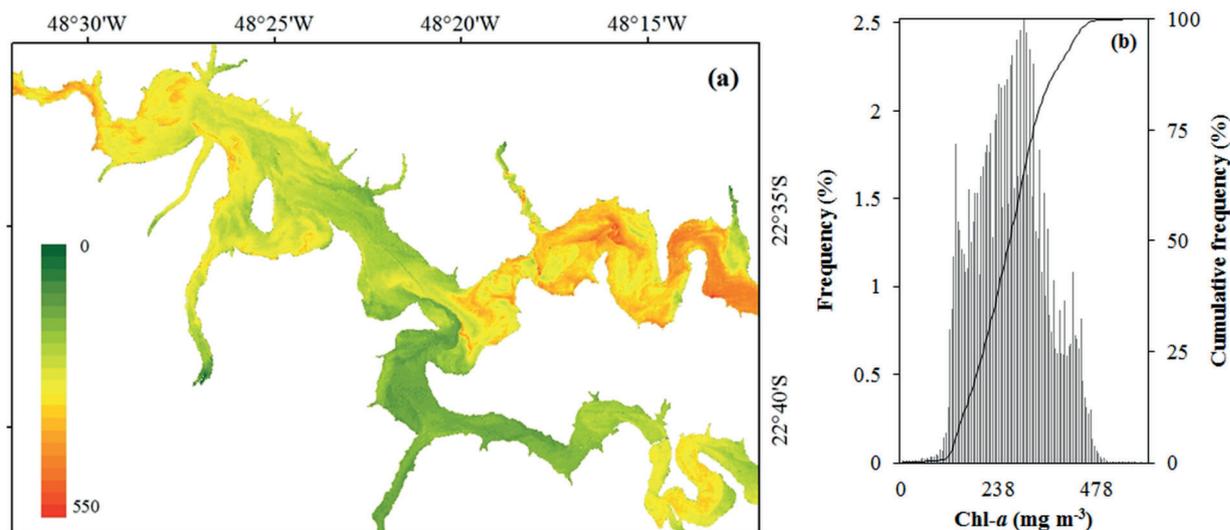
Figure 4 - **(a)** Map of Chl-*a* concentration based on the SLO model using quadratic fit and **(b)** frequency plot of occurrence of Chl-*a* concentrations.

et al. 2016). Therefore, the use of the wavelength at 665 nm, associated with the absorption by Chl-*a*, in models, undergoes influence of pigment packaging. Figure 5 shows the average absorption coefficient of pure water (a_w), a_φ, a_{CDOM}, and a_{NAP}. It is clearly noticed the increase of a_φ and a_{CDOM} from the first field survey to the second one. This increase of absorption might be directly associated with 2014 drought, which led to closing dam and, consequently, accumulation of materials and nutrients for primary production.

The model underestimated strongly the Chl-*a* in Tietê River before confluence with the Piracicaba River. Samples collected in that region were identified as outliers and removed from the calibration of models; hence, the models are not representative of that reservoir region. In other words, these points are not bio-optically similar in relation to the rest of the reservoir. Certainly, the high wastewater load coming from the lower course of the Tietê River is responsible for the singular bio-optical status found in this section. Taking into account the spatial resolution of the OLI sensor (30 m), the SLO model has shown satisfactory results.

The model was sensitive in detecting the changes in water color associated with Chl-*a* concentration variation, although the calibration data were acquired in a GSD (Ground Sampling Distance) much smaller than the image. Analyzing Fig. 5, we noticed a spectral gradient between green and red regions, which was useful to estimate Chl-*a*. In addition, the Slope index highlighted further that gradient, since it determines the rate of spectral variation in that range, differently of simple ratio, in which simply defines how often the absorption at red band is greater than at green band.

CONCLUSIONS

The results obtained in this work showed that the band ratios based on NIR-red algorithms based on Sentinel-2 image presented the best performance for estimating Chl-*a* in BBHR. Probably, the insertion of the reflectance peak at 705 nm was a differential, due to the contrast with maximum absorption in the red region (about 665 nm). Unfortunately, we do not have a Sentinel-2 image matching one of the fieldworks to map the Chl-*a*, because, it will likely produce good results.
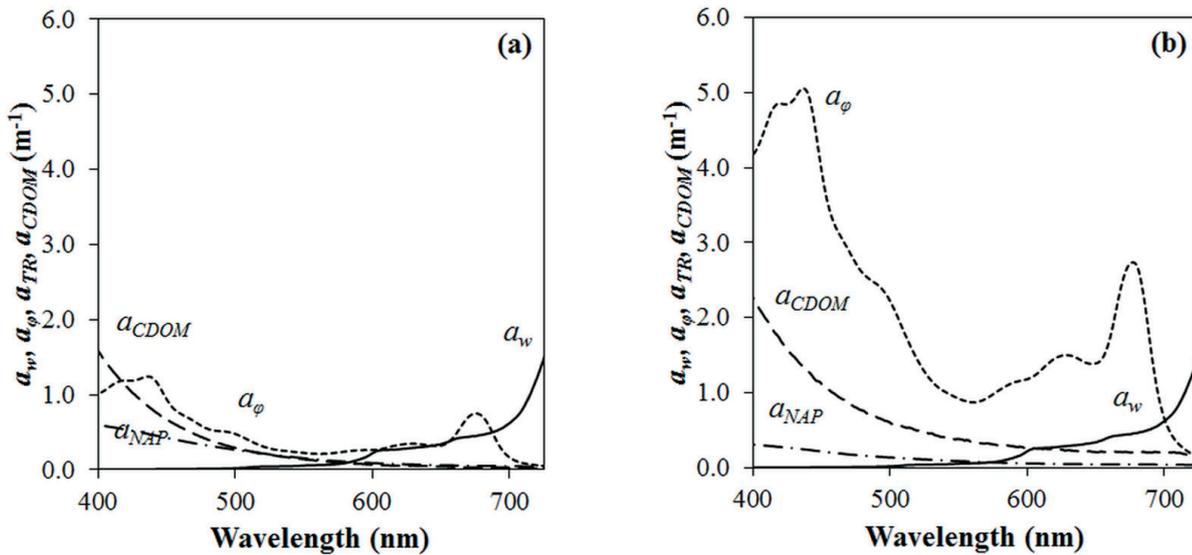
Figure 5 - Average absorption coefficients of pure water (a_w, solid line), phytoplankton (a_φ, dotted line), colored dissolved organic matter (a_{CDOM}, dashed line), and non-algal particles (a_{NAP}, dotted-dashed line) measured in (**a**) May and (**b**) October 2014.

The quadratic SLO model highlighted the difference between the gradient produced by the reflectance peak in the green region and absorption in the red, which the simple ratio (2O) was not able to show. Even though the Slope model has not obtained the best results in validation, it exhibited a satisfactory performance in mapping. The divergent results of fit and mapping with the validation confirm that the empirical models are limited by time. It is also possible that the atypical climate conditions found in 2014 caused the models not to be representative of other years. Below average rainfall required greater flow control in BBHR, increasing time retention, Chl-*a* concentration (greater than 700 mg·m^{-3}) and, consequently, changed the bio-optical status.

Samples collected in the Tietê River before confluence with the Piracicaba River were identified as outliers, due to the singular bio-optical status of this region of the reservoir. The discharge of wastewater coming from the São Paulo metropolitan area is certainly the main responsible for this bio-optical difference. In addition, the pigment packaging showed to interfere strongly in the performance of the Chl-*a* estimation model, since a_φ does not increase proportionally with the elevation of concentration, promoting underestimation of Chl-*a*. Therefore, these results indicate that a unique model cannot be enough to explain the Chl-*a* in the entire reservoir. Thus, the development of regional models must be better investigated where the bio-optical status are partitioned horizontally.

REFERENCES

ADLER-GOLDEN S, BERK A, BERNSTEIN LS, RICHTSMEIER S, ACHARYA PK, MATTHEW MW, ANDERSON GP, ALLRED CL, JEONG LS AND CHETWYND JH. 1998. FLAASH, a MODTRAN4 atmospheric correction package for hyperspectral data retrievals and simulations. Proc 7th JPL Workshop, Pasadena, CA, USA.

AIKEN J, MOORE GF, TREES CC, HOOKER SB AND CLARK DK. 1995. The SeaWiFS CZCS-type pigment algorithm. In: Hooker SB and Firestone ER (Eds), SeaWiFS technical report series, Volume 29. NASA, Goddard Space Flight Center, Greenbelt, MD.

ALCÂNTARA E, WATANABE F, RODRIGUES T AND BERNARDO N. 2016. The phytoplankton packaging effect and the chlorophyll-a specific absorption coefficient in Barra Bonita reservoir, Brazil. Remote Sens Lett 7(8): 761-770.

APHA - AMERICAN PUBLIC HEALTH ASSOCIATION. 1998. AWWA (American Water Works Association), WEF (Water Environmental Federation). Standard methods for the examination of water and wastewater. 20th ed. Washington, DC, USA: APHA, AWWA, WEF, p. 2-54.

BARSI JA, LEE K, KVARAN G, MARKHAM BL AND PEDELTY JA. 2014. The spectral response of the Landsat-8 Operational Land Imager. Remote Sens 6(10): 10232-10251.

BERNARDO N, WATANABE F, RODRIGUES R AND ALCÂNTARA E. 2017. Atmospheric correction issues for retrieving total suspended matter concentrations in inland waters using OLI/Landsat-8 image. Adv Space Res 59(9): 2335-2348.

BRICAUD A, BABIN M, MOREL A AND CLAUSTRE H. 1995. Variability in the chlorophyll-specific absorption coefficients of natural phytoplankton: analysis and parameterization. J Geophys Res 100(13): 321-332.

CARDER KL, CHEN FR, LEE ZP AND HAWES SK. 1999. Semianalytic Moderate-Resolution Imaging Spectrometer algorithms for chlorophyll a and absorption with bio-optical domains based on nitrate-depletion temperatures. J Geophys Res 104(C3): 5403-5421.

CARLSON RE. 1977. A tropical state index for lakes. Limnol Oceanogr 22(2): 361-369.

CIOTTI AM, LEWIS MR AND CULLEN JJ. 2002. Assessment of the relationships between dominant cell size in natural phytoplankton communities and the spectral shape of the absorption coefficient. Limnol Oceanogr 47(2): 404-417.

CLARK DK. 1997. MODIS algorithm theoretical basis document: bio-optical algorithms – case 1 waters, version 1.2. NOAA, Washington, DC.

COELHO CAS ET AL. 2016. The 2014 southeast Brazil austral summer drought: regional scale mechanisms and teleconnections. Clim Dynam 46: 3737-3752.

DALL'OLMO G, GITELSON AA, RUNDQUIST DC, LEAVITT B, BARROW T AND HOLZ JC. 2005. Assessing the potential of SeaWiFS and MODIS for estimating chlorophyll concentration in turbid productive waters using red and near-infrared bands. Remote Sens Environ 96: 176-187.

DANTAS EW, MOURA AN AND BITTENCOURT-OLIVEIRA C. 2011. Cyanobacterial blooms in stratified and destratified eutrophic reservoirs in semi-arid region of Brazil. An Acad Bras Cienc 83: 1327-1338.

ESA - EUROPEAN SPACE AGENCY. 2015. Sentinel-2A spectral response functions (S2A-SRF): COPE-GSEG-EOPG-TN-15-0007.

GETIRANA A. 2016. Extreme water deficit in Brazil detected from space. J Hydrometeorol 17: 591-599.

GITELSON AA, DALL'OLMO G, MOSES W, RUNDQUIST DC, BARROW T, FISCHER TR, GURLIN D AND HOLZ J. 2008. A simple semi-analytical model for remote estimation of chlorophyll-*a* in turbid waters: validation. Remote Sens Environ 112: 3582-3593.

GITELSON AA, GRITZ Y AND MERZLYAK MN. 2003. Relationships between leaf chlorophyll content and spectral reflectance and algorithms for non-destructive chlorophyll assessment in higher plant leaves. J Plant Physiol 160: 271-282.

GOLTERMAN HL. 1975. Developments in water science 2. Physiological limnology: an approach to the physiology of lake ecosystems. Amsterdam, Netherlands: Elsevier.

GOODIN DG, HAN L, FRASER RN, RUNDQUIST DC, STEBBINS WA AND SCHALLES JF. 1993. Analysis of suspended solids in water using remotely sensed high resolution derivative spectra. Photogramm Eng Remote Sens 59(4): 505-510.

GORDON HR, BROWN JW AND EVANS RH. 1988. Exact Rayleigh scattering calculations for use with the Nimbus-7 Coastal Zone Color Scanner. Appl Opt 27(5): 862-871.

LE C, LI Y, ZHA Y, SUN D, HUANG C AND LU H. 2009. A four-band semi-analytical model for estimating chlorophyll a in highly turbid lakes: the case of Taihu Lake, China. Remote Sens Environ 113: 1175-1182.

MANNINO A, RUSS ME AND HOOKER SB. 2008. Algorithm development and validation for satellite-derived distributions of DOC and CDOM in the U.S. Middle Atlantic Bight. J Geophys Res 113(C07051): 1-19.

MATSUMURA-TUNDISI T AND TUNDISI JG. 2005. Phytoplankton richness in a eutrophic reservoir (Barra Bonita reservoir, SP, Brazil). Hydrobiologia 542: 367-378.

MISHRA DR AND MISHRA S. 2010. Plume and bloom: effect of the Mississippi River diversion on the water quality of Lake Pontchartrain. Geocarto Int 25(7): 555-568.

MISHRA S AND MISHRA DR. 2012. Normalized difference chlorophyll index: a novel model for remote estimation of

chlorophyll-a concentration in turbid productive waters. Remote Sens Environ 117: 394-406.

MOBLEY CD. 1999. Estimation of the remote-sensing reflectance from above-surface measurements. Appl Opt 38(36): 7442-7455.

MOSES WJ, GITELSON AA, BERDNKOV S, SAPRYGIN V AND POVAZHNYI V. 2012. Operational MERIS-based NIR-red algorithms for estimating chlorophyll-a concentrations in coastal waters – the Azov Sea case study. Remote Sens Environ 121: 118-124.

MUELLER JL, FARGION GS AND MCCLAIN CR. 2003. Ocean optics protocols for satellite ocean color sensor validation, Revision 4, Volume III: radiometric measurements and data analysis protocols. NASA, Goddard Space Flight Space Center, Greenbelt, MD.

OLIVEIRA FHPC, ARA ALSC, MOREIRA CHP, LIRA OO, PADILHA MRF AND SHINOHARA KS. 2014. Seasonal changes of water quality in a tropical shallow and eutrophic reservoir in the metropolitan region of Recife (Pernambuco-Brazil). An Acad Bras Cienc 86: 1863-1872.

PAHLEVAN N, SCHOTT JR, FRANZ BA, ZIBORDI G, MARKHAM B, BAILEY S, SCHAAF CB, ONDRUSEK M, GREB S AND STRAIT CM. 2017. Landsat 8 remote sensing reflectance (Rrs) products: evaluation, intercomparisons, and enhancements. Remote Sens Environ 190: 289-301.

PRADO RB AND NOVO EMLM. 2015. Modeling pollution potential input from the drainage basin into Barra Bonita reservoir, São Paulo - Brazil. Braz J Biol 75(2): 314-323.

SIEGEL DA, WANG M, MARITORENA S AND ROBINSON W. 2000. Atmospheric correction of satellite ocean color imagery: the black pixel assumption. Appl Opt 39(21): 3582-3591.

TUNDISI JG, MATSUMURA-TUNDISI T AND ABE DS. 2008. The ecological dynamics of Barra Bonita (Tietê River, SP, Brazil) reservoir: implications for its biodiversity. Braz J Biol 68: 1079-1098.

VAN DER MEER F. Physical principles of optical remote sensing. 1999. In: Stein A, Van Der Meer F and Gorte B (Eds), Spatial statistics for remote sensing. Dordrecht, Netherlands, Kluwer Academic Publishers, chapter 3.

VOLLENWEIDER RA AND KEREKES JJ. 1980. Background and summary results of the OECD cooperative program on eutrophication. Proceedings of the International Symposium on Inland Waters and Lake Restoration. U.S. Environmental Protection Agency. EPA 440/5-81-010, p. 25-36.

WATANABE F, ALCÂNTARA EH, RODRIGUES T, IMAI NN, BARBOSA C AND ROTTA L. 2015. Estimation of chlorophyll-a concentration and the trophic state of the Barra Bonita hydroelectric reservoir using OLI/Landsat-8 images. Int J Environ Res Public Health 12: 10391-10417.

WATANABE F, RODRIGUES T, BERNARDO N, ALCÂNTARA E AND IMAI N. 2016. Drought can cause phytoplankton growth intensification in Barra Bonita reservoir. Model Earth Syst Environ 2: 134.